Journal of Alloys and Compounds 513 (2012) 393–398

Contents lists available at SciVerse ScienceDirect

Journal of Alloys and Compounds

journal homepage: www.elsevier.com/locate/jallcom

Improvement of rate capability of spinel lithium titanate anodes using microwave-assisted zinc nanocoating

Chien-Te Hsieh*, Bi-Sheng Chang, Jia-Yi Lin, Ruey-Shin Juang

Department of Chemical Engineering and Materials Science, Yuan Ze Fuel Cell Center, Yuan Ze University, Taoyuan 320, Taiwan

ARTICLE INFO

Article history:
Received 24 May 2011
Received in revised form 6 October 2011
Accepted 16 October 2011
Available online 25 October 2011

Keywords:
$Li_4Ti_5O_{12}$
Li-ion battery
Microwave deposition
Zinc coating
Anode materials

ABSTRACT

In this study, the deposition of microwave-assisted Zn layers onto spinel lithium titanate ($Li_4Ti_5O_{12}$) crystals as superior anode materials for Li-ion batteries has been investigated. Microwave heating is capable of rapidly depositing Zn layers over the surface of spinel $Li_4Ti_5O_{12}$ within 6 min. The thickness of Zn layer (i.e., 1–10 nm) is an increasing function of zinc nitrate concentration under the microwave irradiation. The charge–discharge curve of Zn–$Li_4Ti_5O_{12}$ anode still maintains the plateau at 1.5 V, contributing to the major portion in the overall specific capacity. The presence of Zn coating significantly facilitates the capacity retention (78.1% at 10 *C*/0.2 *C*) of the composite anodes with high Coulombic efficiency (>99.9%), indicating an excellent reversibility of insertion/de-insertion of Li ions. This can be ascribed to the fact that well-dispersed Zn layer offers an electronic pathway over the $Li_4Ti_5O_{12}$ powder, thus imparting electronic conduction and reducing cell polarization. Accordingly, the deposition of Zn coating, prepared by the rapid microwave heating, shows a positive effect on the rate-capability improvement of $Li_4Ti_5O_{12}$ anodes.

1. Introduction

Spinel lithium titanate ($Li_4Ti_5O_{12}$) is an attractive anode material for Li-ion batteries, capable of reversibly intercalating Li ions up to $Li_7Ti_5O_{12}$ [1–3]. Since per formula unit $Li_4Ti_5O_{12}$ can store three Li ions at a stable voltage plateau of approximately 1.5 V vs. Li/Li^+, its theoretical capacity is 175 mAh g^{-1} [4,5]. The favorable electrochemical characteristics of $Li_4Ti_5O_{12}$ are its flat discharge curve and its negligible structural variations upon cycling, i.e., zero strain insertion [7,8]. The spinel structure of $Li_4Ti_5O_{12}$ offers a robust three-dimensional interstitial 8a tetrahedral and 16c octahedral space, allowing the intercalation of Li ions into the $Li_4Ti_5O_{12}$ framework and forming a rock-salt-type $Li_7Ti_5O_{12}$ structure [1]. Thus, the intercalation/de-intercalation of Li ions into the spinel $Li_4Ti_5O_{12}$ is extremely reversible, showing good capacity retention. However, due to its low electronic conductivity, the $Li_4Ti_5O_{12}$ anodes exhibit a poor rate capability. Some conductive additives, such as acetylene black, in the anodes could compensate for the low conductivity. However, too much additives significantly reduce the energy density of $Li_4Ti_5O_{12}$ anodes, thereby hindering the practical use in Li-ion batteries.

To resolve this problem, pioneering studies have aimed at the conductivity improvement of $Li_4Ti_5O_{12}$ powders, such as Cu particles using electrode-less deposition [9] and carbon coating using critic acid sol–gel method [3], sugar-containing impregnation [10], carbonization of resin [11], drop emulsion technique [12], and polyvinylbutyral rheological phase method [13]. Owing to great success, the $Li_4Ti_5O_{12}$ composites have been considered as a potential anode material for high-power Li-ion batteries. This directs us to the development of a novel coating approach on the spinel powders. Several metal oxides, such as MgO and SnO_2, have been observed to improve the high-voltage cycleability of $LiCoO_2$ cathodes. Recently, zinc oxide (ZnO)-coated $LiCoO_2$ and $LiMn_{1.5}Ni_{0.5}O_4$ cathodes have been found to display the capability to retard abrupt capacity fading at high cutoff voltage [14,15]. Chemical wet impregnation, followed by calcination process, is one of the frequently used routes to coat ZnO layers over these cathodes. From the economic viewpoint, microwave-assisted method can be considered as an efficient approach to synthesize inorganic nanostructures due to its simplicity, rapid synthesis, and energy-saving nature [16,17]. Accordingly, this study proposes a facile microwave synthesis of nanosized Zn layer onto spinel $Li_4Ti_5O_{12}$, exhibiting excellent rate capability.

Through microwave-assisted reduction, metallic Zn nanolayers were uniformly attached to the spinel $Li_4Ti_5O_{12}$ powders, thus forming Zn-coated $Li_4Ti_5O_{12}$ composites. The metallic Zn nanolayers with different thicknesses could be obtained by adjusting Zn^{2+} concentration under microwave irradiation. The rapid synthesis enabled the formation of uniform Zn layers in aqueous solution. The Zn-coated $Li_4Ti_5O_{12}$ anodes were systematically characterized by structural analysis and charge–discharge cycling at various *C* rates. To inspect the influence of Zn layer, fresh $Li_4Ti_5O_{12}$ anode

* Corresponding author. Tel.: +886 3 4638800x2577; fax: +886 3 4559373.
E-mail address: cthsieh@saturn.yzu.edu.tw (C.-T. Hsieh).

0925-8388/$ – see front matter © 2011 Elsevier B.V. All rights reserved.
doi:10.1016/j.jallcom.2011.10.055

was also fabricated to compare the cell performance. The aim of this study was to shed some light on how the deposition of Zn layer on the spinel structures offers a pathway for Li^+ intercalation/de-intercalation, imparting high rate capability and excellent cyclic stability. This satisfactory result is beneficial for the development of $Li_4Ti_5O_{12}$ anodes in practical use of Li-ion batteries.

2. Experimental

Virginal $Li_4Ti_5O_{12}$ was prepared by sintering a stoichiometric amount of LiOH (Aldrich) and TiO_2 (P25, Degussa Co.) at 850 °C in air for 12 h. The molar ratios of Li:Ti was set at 4.2:5, and the precursor was mixed with distilled water by rotary ball milling at a speed of 300 rpm for 4 h to form slurry. The solid-state reaction enabled the formation of spinel $Li_4Ti_5O_{12}$ powders. One-stage procedure of microwave-assisted polyol synthesis for depositing Zn layers on the $Li_4Ti_5O_{12}$ can be described as follows. The as-derived $Li_4Ti_5O_{12}$ powders were impregnated with a Zn-containing solution in a beaker. The ionic solution consisted of 1 ml of 0.05 M $Zn(NO_3)_2$, 1 ml of 0.04 M KOH, and 30 ml of ethylene glycol. The beaker was then placed at the center of a household microwave oven and then heated for 6 min under microwave power of 720 W. The metal-coated $Li_4Ti_5O_{12}$ samples were then separated from the solution and dried at 105 °C in a vacuum oven overnight. The Zn^{2+} concentration was chosen to control the thickness of Zn layer over the $Li_4Ti_5O_{12}$ powders. The other two ionic solutions (i.e., 0.1 and 0.2 M $Zn(NO_3)_2$) were separately prepared and then added into each aqueous solution. Subsequently, the microwave-assisted depositions were carried out under the same operating condition.

Field-emission scanning electron microscope (FE-SEM, JEOL 2010F) and high-resolution transmission electron microscope (HR-TEM, JEOL, JEM-2100) were adopted to observe the morphology of $Li_4Ti_5O_{12}$ powders. The chemical composition of the as-grown powders was characterized using inductively coupled plasma-atomic emission spectrometry (ICP-AES) and analyzed using X-ray photoelectron spectroscopy (XPS). The XPS spectra were recorded with a Fison VG ESCA210 spectrometer and Mg Kα radiation. The crystalline structure of $Li_4Ti_5O_{12}$ samples was characterized by X-ray diffraction (XRD) with Cu Kα radiation, using an automated X-ray diffractometer (Shimadzu Labx XRD-6000).

The electrochemical measurements of $Li_4Ti_5O_{12}$ powders were examined by coin cell testing. The $Li_4Ti_5O_{12}$ powders were added into a solution of polyvinylidenefluoride (PVdF) in N-methyl pyrrolidinone (NMP), and the mixtures were blended by a 3D mixer using zirconia balls for 3 h to prepare uniform slurries. All electrodes were prepared by pressing the slurry on copper foils with a doctor blade, followed by evaporating the solvent, NMP, with a blower dryer. The electrode layers, consisting of 85 wt.% $Li_4Ti_5O_{12}$ active material, 10 wt.% PVdF binder, 2 wt.% Super-P, and 3 wt.% KS-6 were adjusted to have a thickness of 100 μm. The Super-P and KS-6 served as a conductive agent. In the test cells, Li metal and porous polypropylene film was used as counter electrode and separator, respectively. The electrolyte solution was 1.0 M $LiPF_6$ in a mixture of ethylene carbonate, polycarbonate, and dimethyl carbonate, with a weight ratio of 3:2:5. The charge/discharge cycling test at various *C* rates (from 0.2 to 10 *C*) was performed within the voltage region of 1–3 V vs. Li/Li^+ at ambient temperature.

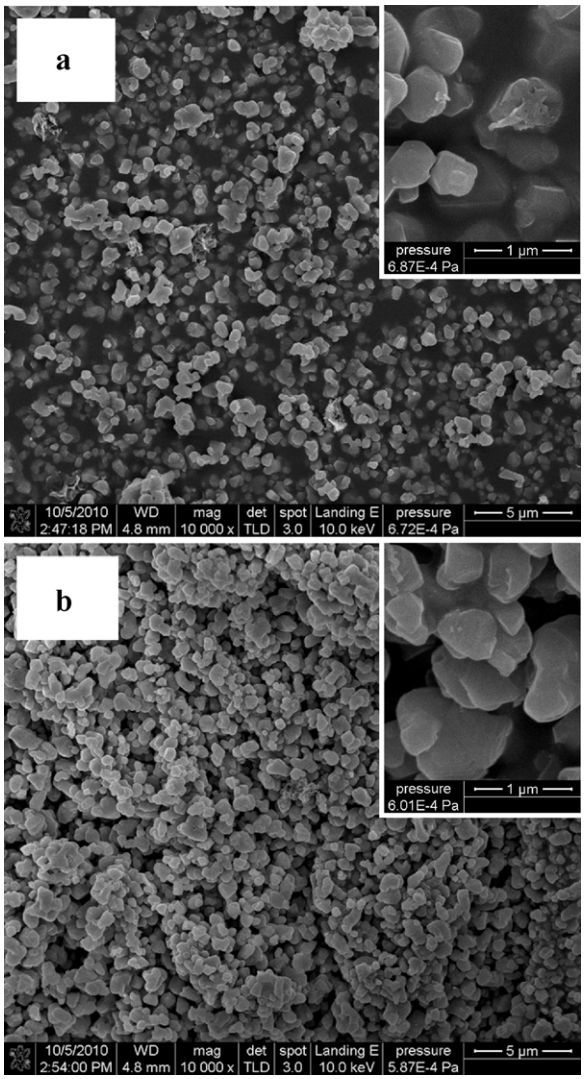

Fig. 1. FE-SEM images of (a) pristine and (b) Zn-coated $Li_4Ti_5O_{12}$ powders, in which the insets are high-magnification FE-SEM images.

3. Results and discussion

Fig. 1(a) shows the FE-SEM image of original $Li_4Ti_5O_{12}$ powders sintered at 850 °C for 12 h. The particles appear to have cubic shape, and the particle size ranges from 300 nm to 1 μm. After microwave heating, Zn-coated $Li_4Ti_5O_{12}$ powders were found to retain the original morphology, as shown in Fig. 1(b). The modified sample was still found to be composed of fine particles of submicron size. HR-TEM micrographs on as-prepared $Li_4Ti_5O_{12}$ powder in the presence of 0.05 and 0.2 M Zn^{2+} solutions under the microwave irradiation are illustrated in Fig. 2(a) and (b), respectively. The images clearly illustrate that a thin Zn layer is deposited over the particles. The thickness of the Zn nanocoating evidently depends on the Zn ionic concentration, and the average thicknesses are 1–2 and 5–10 nm after microwave-assisted deposition in 0.05 and 0.2 M Zn^{2+} solutions, respectively. As a result, the Zn^{2+} concentration is capable of adjusting the coating thickness over the spinel powders under microwave irradiation. The ICP-AES approach was adopted to inspect the chemical composition of the layer, confirming the presence of Zn element. However, Zn and O elements are detected at interface between the Zn layer and the spinel crystal, possibly originated from the spinel and partially oxidized Zn layer.

XPS was used to analyze the chemical composition of Zn-coated $Li_4Ti_5O_{12}$ powder, as shown in Fig. 3. This powder was prepared in the presence of 0.2 M Zn^{2+} solutions under microwave irradiation. The Ti 2p, O 1s, Zn 2p peaks of the scan spectra have binding energies of *ca.* 458.9, 531.5, and 1021.1 eV, respectively. The atomic ratios of Zn for the three types of Zn-coated $Li_4Ti_5O_{12}$ samples are found to be 0.54, 1.21, and 2.08%, which is in agreement with the order of Zn^{2+} ionic concentration. This increase in the atomic ratio is attributed to more Zn^{2+} ions adsorbed onto the spinel powders in high concentration. The adsorption capacity of Zn^{2+} significantly influences the Zn surface composition on $Li_4Ti_5O_{12}$ powders after microwave deposition. It can be seen from the inset of Fig. 3 that the peak appearing at the binding energy of 1021.1 eV, which can be assigned to Zn $2p_{3/2}$ peak, indicates the element Zn in a state of Zn^0 [18]. Spin–orbit splitting is the difference between the binding-energy values of Zn $2p_{3/2}$ and Zn $2p_{1/2}$ levels. The observed spin–orbit splitting was ~23.09 eV [19], confirming the presence of metallic Zn layers over the spinel powders.

The schematic diagram for growing Zn layers is illustrated in Fig. 4. This mechanism consists of two steps: (i) ionic adsorption and (ii) microwave-assisted reduction. The ionic adsorption would take place on the surface of spinel $Li_4Ti_5O_{12}$ powder in the liquid phase. The adsorption capacity is generally an increasing function of the equilibrium concentration. The spinel $Li_4Ti_5O_{12}$ offers a number of adsorptive sites, available for the adsorption

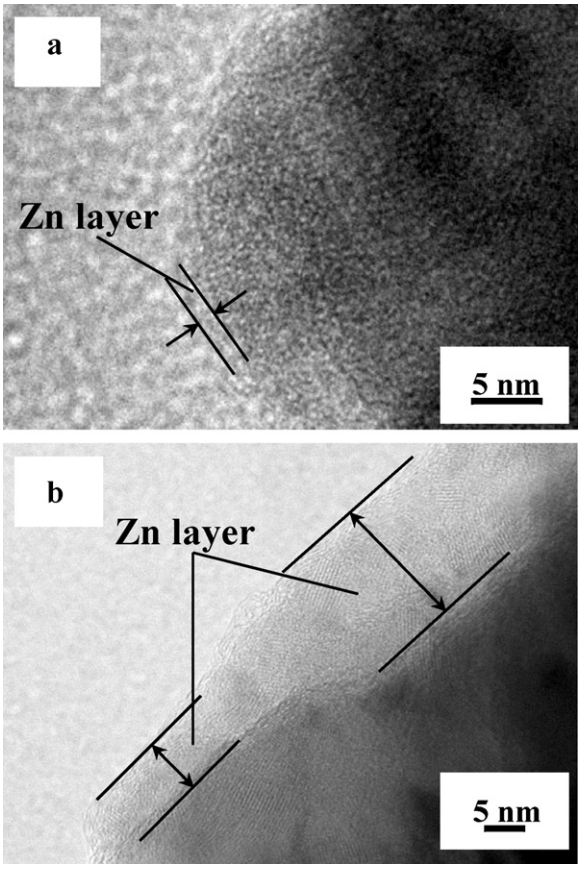

Fig. 2. HR-TEM images for Zn-coated $Li_4Ti_5O_{12}$, prepared by the microwave-assisted method using (a) 0.05 M and (b) 0.2 M Zn^{2+} concentrations.

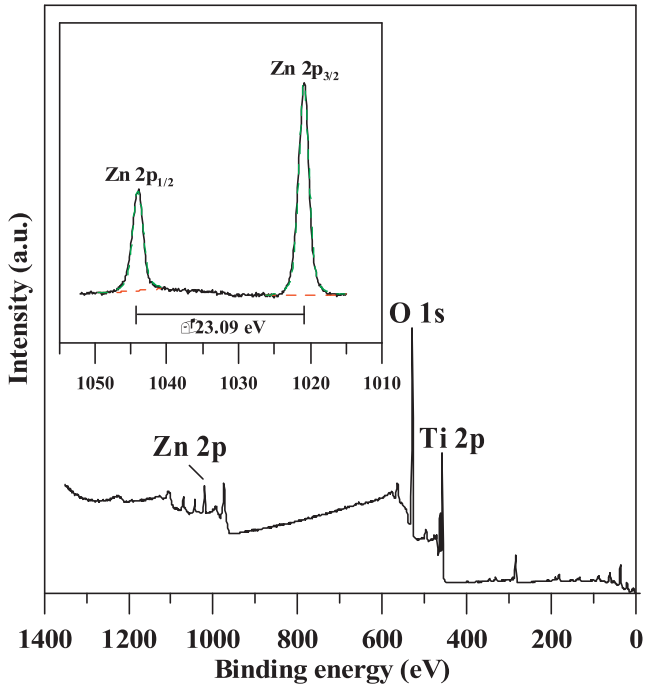

Fig. 3. XPS survey spectrum of Zn-coated $Li_4Ti_5O_{12}$ powders using 0.2 M Zn^{2+} concentration. The inset shows the spectrum of Zn 2p peak.

of Zn^{2+} ions. At a higher concentration, sites that are more vacant would be occupied by the ions, inducing a higher surface coverage or multilayer adsorption. Under microwave irradiation, the microwave energy is adsorbed by the reactant and heating medium, and thus, uniform and rapid heating could be obtained [16]. Thus, high temperature required in chemical reduction can be achieved within 6 min, inducing the deposition of Zn nanolayer. Through microwave heating, the Zn^{2+}-adsorbed layer contributes to the primary layer on the surface of $Li_4Ti_5O_{12}$ powder. Subsequently, the other ions in the bulk solution easily diffuse and then occupy the active sites, resulting from mass transfer. This transport phenomenon becomes more evident at high Zn^{2+} ionic concentration due to the concentration gradient. Therefore, the secondary layer is gradually formed, leading to a thicker layer, especially at high concentration.

Typical XRD patterns of original and Zn-coated $Li_4Ti_5O_{12}$ samples are shown in Fig. 5(a)–(d). The peaks at 2θ angles of 18.3°, 35.6°, 43.2°, 57.2°, and 62.9° are assigned to (1 1 1), (3 1 1), (4 0 0), (4 3 2), (3 3 3), and (4 4 0) representative peaks of spinel $Li_4Ti_5O_{12}$, respectively. This apparently proves the presence of spinel $Li_4Ti_5O_{12}$ crystallites with *Fd*3*m* space group [20,21]. As shown in Fig. 6, spinel $Li_4Ti_5O_{12}$ structure is cubic with eight AB_2X_4 units per unit cell, in which Li ions are located at (8a) tetrahedral sites, Ti ions at (16d) octahedral sites, and oxygen ions at (32e) sites. The spinel solid solution $Li_4Ti_5O_{12}$ is able to undergo reversible Li insertion/de-insertion up to the composition $x = 3$ in $Li_{4+x}Ti_5O_{12}$ [4,22]. As the Zn layer is very thin, it is difficult to detect such low solid content of <5%, resulting in no Zn reflections observed in the XRD patterns.

Fig. 7(a) and (b) shows the charge–discharge curves of fresh and Zn-coated $Li_4Ti_5O_{12}$ (0.2 M Zn^{2+}) anodes at various *C* rates, respectively. The charge–discharge cycling was performed within the potential ranging from 1 and 3 V vs. Li/Li^+. Both the anodes typically exhibit a similar profile, composed of a quick voltage drop from 3 to ~1.5 V at an initial stage, a first plateau at about 1.5–1.6 V, and a sharp drop from ~1.5 to 1 V. The plateau is the characteristic charge–discharge behavior of spinel $Li_4Ti_5O_{12}$, which is assigned to the insertion/de-insertion of Li ions. The redox reaction can be

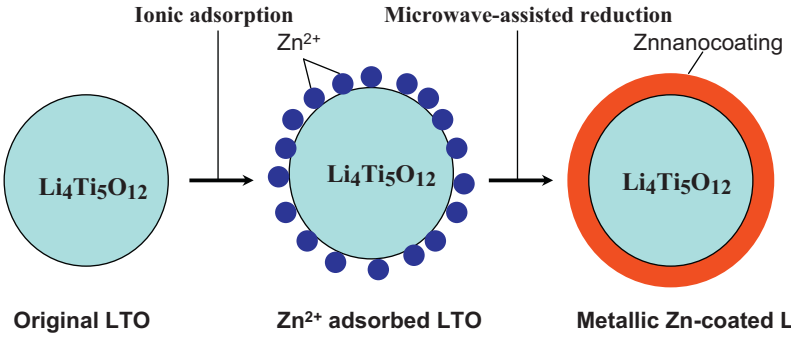

Fig. 4. Schematic diagram for growing Zn coating over $Li_4Ti_5O_{12}$ (LTO) powder by the microwave-assisted synthesis.

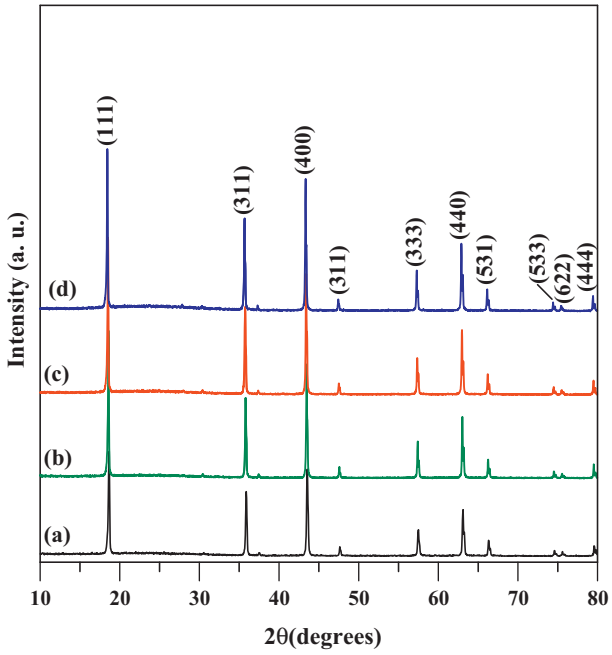

Fig. 5. Typical XRD patterns of different $Li_4Ti_5O_{12}$ powders: (a) pristine $Li_4Ti_5O_{12}$ and Zn-coated $Li_4Ti_5O_{12}$ by microwave-assisted method using (b) 0.05, (c) 0.1, and (d) 0.2 M Zn^{2+} concentrations.

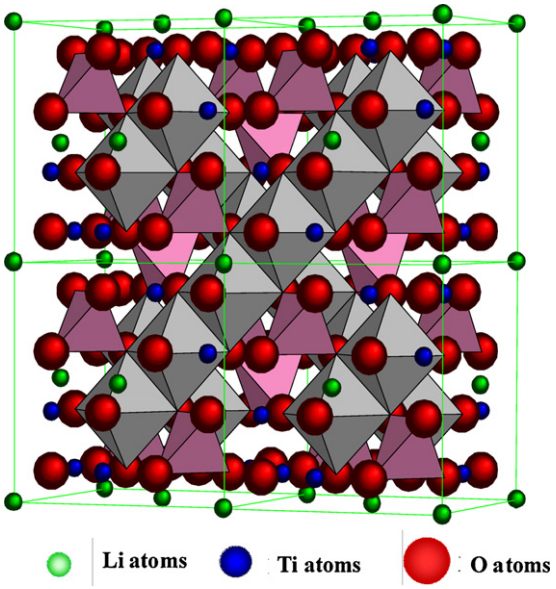

Fig. 6. Crystal structures of spinel $Li_4Ti_5O_{12}$. Pink tetrahedra represent (8a) sites, gray octahedra represent (16c) sites.

formulated as follows [4,23]:

$$Li_{3(8a)}[LiTi_5{}^{4+}]_{(16d)}O_{12(32e)} + 3e^- + 3Li^+ \leftrightarrow Li_{6(16c)}[LiTi_3{}^{3+}Ti_2{}^{4+}]_{(16d)}O_{12(32e)} \quad (1)$$

The reversible reaction usually takes place at ~1.5 vs. Li/Li^+, and 3 mol Li ions are capable of being inserted into the octahedral (16c) sites of $Li_4Ti_5O_{12}$ lattices, generating a rock-salt structure [1,20]. On the basis of a spinel ↔ NaCl phase transition, almost no volume expansion appears in the Li^+ insertion-extraction process [6,24].

Data from Fig. 7, the discharge capacities of fresh and Zn-coated $Li_4Ti_5O_{12}$ anodes are found to be 175 and 183 mAh g^{-1} at 0.2 *C*, respectively. The charge–discharge curves seem to be

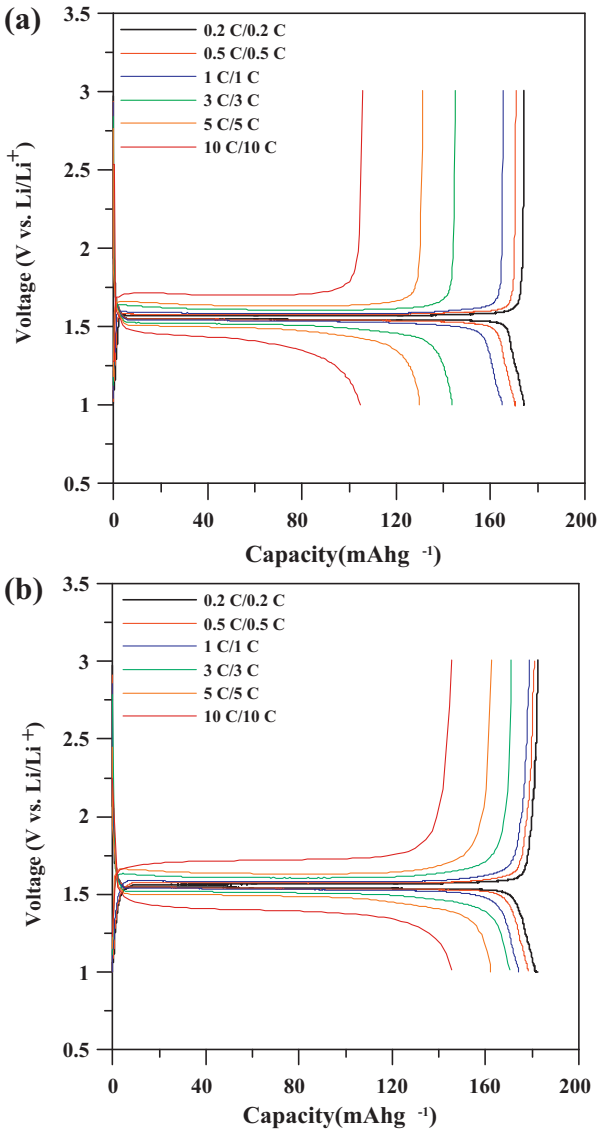

Fig. 7. Typical charge/discharge curves of (a) pristine and (b) Zn-coated $Li_4Ti_5O_{12}$ (0.2 M Zn^{2+} concentration) anodes at different *C* rates.

symmetric, indicating the reversibility of Li^+ intercalation/de-intercalation at low *C* rate. As expected, it can be observed that all discharge capacities decrease with the *C* rate. This can be attributed to the fact that Li^+ diffusion and electron conductions through the spinel layer dominate the charge–discharge process. Fig. 8 depicts the capacity retention for all anodes, based on the ratio of discharge capacity at different *C* rates to 0.2 *C*. Both the anodes were found to exhibit good capacity retention (>96.6%) at the ratio of discharge capacity of 0.5 *C*/0.2 *C*. Furthermore, the original anode exhibited a poor rate capability, whereas Zn-coated $Li_4Ti_5O_{12}$ anode displayed excellent capacity retention at high *C* rate. At the rate of 10 *C*, the ratios of discharge capacity at 10 *C*/0.2 *C* demonstrated the following order: 78.1% (0.2 M Zn^{2+}) > 55.2% (original anode). On the basis of the above-mentioned result, the Zn nanocoating has a positive role in enhancing the rate capability of spinel anodes. This can be attributed to the fact that as pristine $Li_4Ti_5O_{12}$ anode exhibits very low electronic conductivity, proper dispersion of metallic Zn layer obviously is capable of creating an electronic pathway over the $Li_4Ti_5O_{12}$ powder. This surrounding circuit facilitates the electronic conduction and reduces cell polarization, thus inducing the rate capability at high current density. This result is similar to

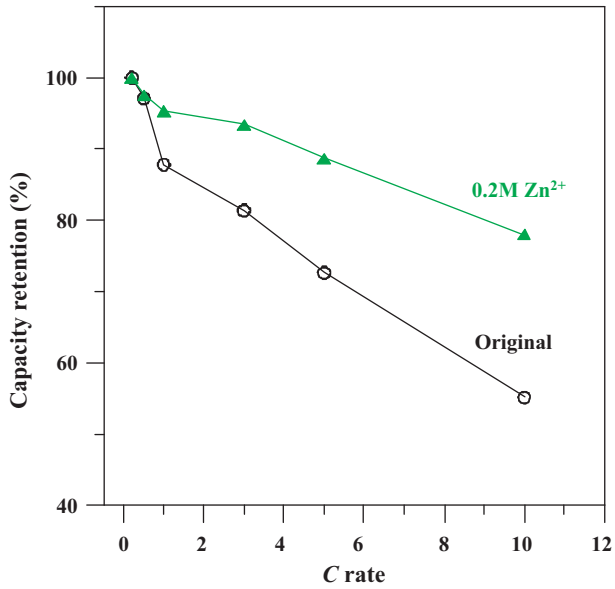

Fig. 8. Discharge capacity retention as a function of *C* rates.

that observed in pioneer studies, such as Ag/$Li_4Ti_5O_{12}$ [25,26] and Cu/$Li_4Ti_5O_{12}$ anodes [9]. As the microwave-assisted deposition only takes a short period (i.e., 6 min in this study), this approach offers a promising potential in the preparation of core–shell anode materials owing to its simplicity and rapid synthesis.

The stability of the prepared anodes was examined by conducting repeated charge–discharge cycling. These coin cells equipped with $Li_4Ti_5O_{12}$ anodes were charged and discharged between 1 and 3 V at different *C* rates to confirm the stability. The discharge capacity as a function of *C* rate is depicted in Fig. 9. The rate capability of the anodes was strongly improved with increasing thickness of Zn layers. Since the Zn layer is well coated over the surface of spinel anode, it can be suggested that Li ions should diffuse through the resultant metallic layer first, followed by the spinel crystals. It is generally recognized that Li transport through spinel regions is difficult, while Li transport through rock-salt regions is relatively easier [27,28], i.e., different diffusion coefficients in lithiated and delithiated states. Based on the result of rate capability, this reflects

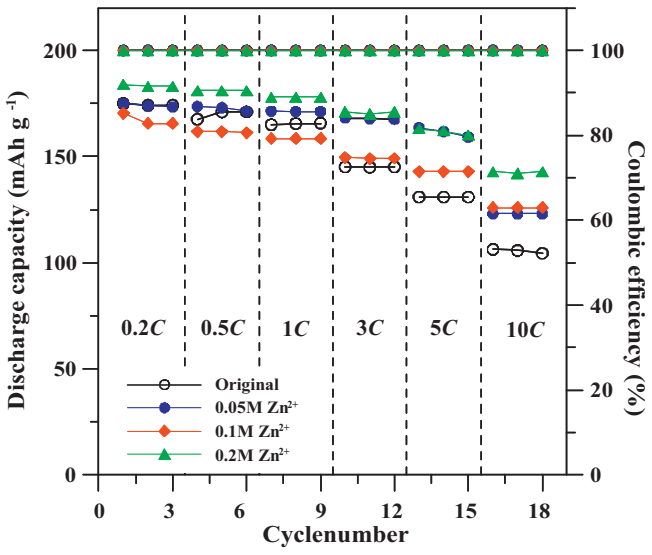

Fig. 9. Discharge capacity and Coulombic efficiency as a function of cycle number at different *C* rates.

the resultant Zn layer does not alter the Li^+ diffusion rate during the lithiated/delithiated process. Thus, the insertion/de-insertion of Li ions enables easily penetration through the Zn layers, showing high transport accessibility. Accordingly, the Zn layer, having an average thickness of 5–10 nm, could not only impart the electronic conduction but also maintain the diffusion rate in the composite anodes. However, this still requires a deeper investigation to figure out the optimal thickness of Zn layer over the spinel crystals.

Fig. 9 also shows the Coulombic efficiency (η) of an anode as a function of cycle number. The η values can be calculated from the following equation:

$$\eta = \frac{t_D}{t_C} \times 100 \quad (2)$$

where t_D and t_C are the times required for discharge and charge, respectively. It has been observed that the Coulombic efficiencies maintain a high value of >99.9% after potential cycling, indicating an excellent reversibility of Li insertion/de-insertion. Again, this finding demonstrates that the deposition of Zn layers on the spinel anodes keeps a smooth pathway for ionic transportation. During the charge–discharge process, the Li ions can easily diffuse through the Zn layer and then intercalate the spinel $Li_4Ti_5O_{12}$ crystals, i.e., no more Li ions are trapped in the spinel crystals, thus leading to high reversibility. Even at high *C* rate (e.g., 10 *C*), the ionic diffusion resistance in the Zn layer is still negligible. This can be attributed to the fact that the microwave-assisted deposition is able to uniformly coat the metallic layers in nanoscale. On the basis of the result, such a design of Zn-coated $Li_4Ti_5O_{12}$ structure displays promising feasibility for anode materials in high-power Li-ion batteries.

4. Conclusions

In this study, we have demonstrated the improvement of rate capability on the $Li_4Ti_5O_{12}$ anodes coated with Zn nanolayers prepared using the microwave-assisted route. The spinel $Li_4Ti_5O_{12}$ powders attached to different thicknesses of Zn layers were prepared by adjusting the ionic concentration under microwave irradiation. As confirmed by HR-TEM observation, the thickness of Zn layer over the spinel anodes was an increasing function of the ionic concentration. The charge–discharge curve of Zn–$Li_4Ti_5O_{12}$ anode still maintained the plateau at 1.5 V, contributing to the major portion in the overall specific capacity. The presence of Zn coating significantly improved the high rate capability (~10 *C*) of the composite anodes with high Coulombic efficiency, indicating good reversibility of Li^+ insertion/de-insertion. This Zn-based surrounding circuit facilitated electronic conduction and reduced cell polarization, thus inducing rate capability at a high rate. In this work, the highest ratio of discharge capacity at 10–0.2 *C* could be reached, i.e., 78.1%, through microwave heating in 0.2 M Zn^{2+} solution. Based on the above-mentioned result, it can be concluded that microwave-assisted synthesis provides an efficient route for the rate-capability improvement of spinel anodes for Li-ion batteries, which is simple, convenient, and time-saving.

Acknowledgements

The authors are very grateful for the financial support from the National Science Council of the Republic of China under the contracts NSC 99-2632-E-155-001-MY3.

References

[1] M. Wagemaker, E.R.H. Eck Van, A.P.M. Kentgens, F.M. Mulder, J. Phys. Chem. B 113 (2009) 224.
[2] F. Ronci, P.E. Stallworth, F. Alamgir, T. Schiros, J. Sluytman, X. Guo, P. Reale, S. Greenbaum, M. denBoer, B. Scrosati, J. Power Sources 119 (2003) 631.
[3] J. Wang, X.M. Liu, H. Yang, X.D. Shen, J. Alloys Compd. 509 (2011) 712.

[4] H. Ge, N. Li, D. Li, C.S. Dai, D.L. Wang, J. Phys. Chem. C 113 (2009) 6324.
[5] E.M. Sorensen, S.J. Barry, H.K. Jung, J.R. Rondinelli, J.T. Vaughey, K.R. Poeppelmeier, Chem. Mater. 18 (2006) 482.
[6] L. Aldon, P. Kubiak, M. Womes, J.C. Jumas, J. Olivier-Fourcade, J.L. Tirado, J.I. Corredor, C. Perez Vicente, Chem. Mater. 16 (2004) 5721.
[7] K. Kataoka, Y. Takahashi, N. Kijima, H. Hayakawa, J. Akimoto, K. Ohshima, Solid State Ionics 180 (2009) 631.
[8] P. Reale, S. Panero, F. Ronci, V. Rossi Albertini, B. Scrosati, Chem. Mater. 15 (2003) 3437.
[9] S. Huang, Z. Wen, B. Lin, J. Han, X. Xu, J. Alloys Compd. 457 (2008) 400.
[10] G.J. Wang, J. Gao, L.J. Fu, N.H. Zhao, Y.P. Wu, T. Takamura, J. Power Sources 174 (2007) 1109.
[11] H. Yu, X. Zhang, A.F. Jalbout, X. Yan, X. Pan, H. Xie, R. Wang, Electrochim. Acta 53 (2008) 4200.
[12] H.E. Park, I.W. Seomg, W.Y. Yoon, J. Power Sources 189 (2009) 499.
[13] H. Liu, Y. Feng, K. Wang, J. Xie, J. Phys. Chem. Solid 69 (2008) 2037.
[14] T. Feng, J.G. Duh, Surf. Coat. Technol. 201 (2006) 1886.
[15] R. Singhal, M.S. Tomar, J.G. Burgos, R.S. Katiyar, J. Power Sources 183 (2008) 334.
[16] G. Yang, G. Wang, W. Hou, J. Phys. Chem. B 109 (2005) 11186.
[17] J. Li, Y.L. Jin, X.G. Zhang, H. Yang, Solid State Ionics 178 (2007) 1590.
[18] B. Zhang, H.B. Zhou, E.H. Han, W. Ke, Electrochim. Acta 54 (2009) 6598.
[19] C.D. Wagner, W.M. Riggs, L.E. Davis, J.F. Moulder, G.F. Muilenberg, Handbook of X-ray Photoelectron Spectroscopy, 1979.
[20] F. Ronci, P. Reale, B. Scrosati, S. Panero, V. Rossi Albertini, P. Perfetti, M. di Nichiel, J.M. Merino, J. Phys. Chem. B 106 (2002) 3082.
[21] L. Aldon, P. Kubiak, M. Womes, J.C. Jumas, J. Olivier-Fourcade, J.L. Tirado, J.I. Corredor, C. Pérez Vicente, Chem. Mater. 16 (2004) 5721.
[22] C.T. Hsieh, J.Y. Lin, J. Alloys Compd. 560 (2011) 231.
[23] X.L. Yao, S. Xie, H.Q. Nian, C.H. Chen, J. Alloys Compd. 465 (2008) 375.
[24] P. Kubiak, A. Garcia, M. Womes, L. Aldon, J. Olivier-Fourcade, P.-E. Lippens, J.-C. Jumas, J. Power Sources 119–121 (2003) 626.
[25] S.H. Huang, Z.Y. Wen, X.J. Zhu, Z.H. Gu, Electrochem. Commun. 6 (2004) 1093.
[26] S.H. Huang, Z.Y. Wen, X.J. Zhu, Z.H. Gu, X.H. Xu, Solid State Ionics 117 (2004) 851.
[27] Y.C. Chen, C.Y. Ouyang, L.J. Song, Z.L. Sun, Electrochim. Acta 56 (2011) 6084.
[28] Y.K. Sun, D.J. Jung, Y.S. Lee, K.S. Nahm, J. Power Sources 125 (2004) 242.